Case Studies in Thermal Engineering 6 (2015) 238–250

Contents lists available at ScienceDirect

Case Studies in Thermal Engineering

journal homepage: www.elsevier.com/locate/csite

Optimization of SiO_2 nanoparticle mass concentration and heat input on a loop heat pipe

Prem Gunnasegaran [a,*], Mohd Zulkifly Abdullah [b], Mohd Zamri Yusoff [a], Siti Fazlili Abdullah [a]

[a] Centre for Fluid Dynamics (CFD), College of Engineering, Universiti Tenaga Nasional, Putrajaya Campus, Jalan IKRAM-UNITEN, 43000 Kajang, Malaysia
[b] School of Aerospace Engineering, Universiti Sains Malaysia, Engineering Campus, 14300 Nibong Tebal, Penang, Malaysia

ARTICLE INFO

Article history:
Received 7 July 2015
Received in revised form
1 October 2015
Accepted 18 October 2015
Available online 20 October 2015

Keywords:
Loop heat pipe
Nanofluid
Optimization
Thermal resistance

ABSTRACT

This study presents the effect of nanoparticle mass concentration and heat input based on the total thermal resistance (R_{th}) of loop heat pipe (LHP), employed for PC-CPU cooling. In this study, silica nanoparticles (SiO_2) in water with particle mass concentration ranged from 0% (pure water) to 3% is considered as the working fluid within the LHP. The experimental design and optimization is accomplished by the design of experimental tool, Response Surface Methodology (RSM). The results show that the nanoparticle mass concentration and the heat input have significant effect on the R_{th} of LHP. For a given heat input, the R_{th} is found to decrease with the increase of the nanoparticle mass concentration up to 0.5% and increased thereafter. It is also found that the R_{th} is decreased when the heat input is increased from 20 W to 60 W. The results are optimized with the objective of minimizing the R_{th}, using Design-Expert software, and the optimized nanoparticle mass concentration and heat input are 0.48% and 59.97 W, respectively, the minimum R_{th} being 2.66 (°C/W). The existence of an optimum nanoparticle mass concentration and heat input are the predominant factors for the improvement in the thermal performance of nanofluid-charged LHP.

1. Introduction

As a new kind of heat transfer working fluid, the nanofluid is a new technology attempt to use the special properties of this functional fluid to enhance the phase-change heat transfer in heat pipes, and will have wide application prospect. The term 'nanofluid' refers to a two-phase mixture with its continuous phase being generally a liquid and the dispersed phase constituted of 'nanoparticles' i.e., extremely fine metallic particles of size below 100 nm. As known, water has been widely used as industrial heat transfer fluid for a long time, but due to higher thermal conductivities of metals compared to water, suspensions of nano-sized solid particles especially metal or metallic oxides particles in water, have been used as heat transfer fluid with higher thermal conductivities. Due to this fact, many studies on various water-based nanofluids have been carried out in the past years [1]. For example, application of water-based nanofluids in a heat exchanger exhibits an increased heat transfer coefficient compared to pure water [2,3]. Seyf and Feizbakhshi [4] study on a numerical investigation of the application of CuO-water nanofluids in micro-pin-fin heat sinks and found a significant enhancement in heat transfer. Hajmohammadi et al. [5] consider Cu and Ag water based nanofluids for the flow and heat transfer of nanofluids over a

* Corresponding author.
E-mail address: prem@uniten.edu.my (P. Gunnasegaran).

http://dx.doi.org/10.1016/j.csite.2015.10.004

Nomenclature

A	area, m^2
A_B	area of base plate, m^2
A_f	surface area of aluminum rectangular fin, m^2
A_h	cross-sectional area of LHP, m^2
C_p	specific heat, J/kg K
L_C	condenser section length, mm
L_E	evaporator section length, mm
L_L	liquid line length, mm
L_V	vapor line length, mm
Q	heat input, W
q	heat flux, W/m^2
Q^*	coolant flow rate, m^3/s
R	thermal resistance, °C/W
R_B	base thermal resistance, °C/W
R_C	convective thermal resistance, °C/W
R_E	evaporator thermal resistance, °C/W
R_V	vapor line thermal resistance, °C/W
R_L	liquid line thermal resistance, °C/W
R_{th}	total thermal resistance, °C/W
T	temperature, °C
t	time, s
T_A	ambient temperature, °C
T_B	base plate temperature, °C
T_C	condenser temperature, °C
T_E	evaporator temperature, °C
T_V	vapor line temperature, °C
T_L	liquid line temperature, °C

Greek symbols

μ	dynamic viscosity, Ns/m^2
ρ	density, kg/m^3
φ	particle mass concentration, %

Subscripts

bf	base fluid
nf	nanofluid
s	solid
w	wall

permeable flat plate with convective boundary condition. In the cases of injection and impermeable surface, increasing the nanoparticles volume fraction result in augmentation of convection heat transfer rate. However, in the case of suction, adding Cu and Ag particles reduces the convection heat transfer coefficient at the surface. Overall, many researchers have been devoted to exploiting water-based nanofluids. A comprehensive review of studies on various heat pipes utilizing water-based nanofluids as working fluids in recent years has been presented in Table 1. The research on application of nanofluids in heat pipes was firstly published in 2003 [6]. Over 37 relevant articles have been published since then as shown in Table 1, involving micro-grooved heat pipe, mesh wick heat pipe, sintered metal wick heat pipe, oscillating heat pipe (OHP), and loop heat pipe (LHP). The applied nano-materials included metal, metal oxides, diamond, carbon nanotubes and several other materials.

The fundamental studies of nanofluids applied in heat pipes are still in its initial stage, most of research works are carried out experimentally to focus on finding out key factors affecting the reliable application of nanofluids in the heat pipes and some experimental results cannot be unified yet. The type, size of heat pipes and operating conditions of heat pipes, the kind of base fluids, the material and size of nanoparticles all varied in very wide ranges among these experiments. Therefore, it is difficult to quantitatively make the comparison among different experimental data and then the most existing research conclusions are qualitative. Moreover, study on optimization of operating parameters is also rare.

Results of the limited number of available references have shown that nanofluids have great application prospects in various heat pipes. For the majority of micro-grooved heat pipes, mesh wick heat pipe and oscillating heat pipes, adding nanoparticles to the base fluid can significantly enhance the heat transfer, reduce the total thermal resistance and increase the maximum heat removal capacity. At the same time, there are still some problems such as the stability of nanofluid and challenges on the mechanisms of the heat transfer enhancement and the actual applications. The application of nanofluids must be properly investigated in order to better identify the constraints and issues related to the use of nanofluids in heat pipes.

Nevertheless, most of the previous works considered on conventional heat pipes such as micro-grooved heat pipe, mesh wick heat pipe and oscillating heat pipe, and there is far less work conducted for LHPs. As LHPs are demonstrated to be a reliable and great potential for electronic cooling applications, the use of nanofluids could represent a gain in their performance simply by adding a certain volume of nanoparticles to the working fluid. Furthermore, since LHPs utilize the phase change of the working fluid to transport the heat, the selection of nanofluid is of essential importance to promote the thermal performance of LHPs. Due to only few studies on thermal performance of LHP charged with nanofluid has been reported in the past, more investigations are needed. Accordingly, in the present research, all the aforementioned issues on application of nanofluid in LHP are addressed experimentally and the results are optimized with the objective of minimizing the total thermal resistance (R_{th}) of LHP charged with nanofluid, using Design-Expert software. The results presented establish the existence of an optimum concentration of nanoparticles within the working fluid with respect to attaining the maximum heat transfer.

Table 1
Summary of researchers of heat pipes using nanofluids.

Type of heat pipe	Researcher	Working nanofluid type (nanoparticle size and mass concentration)	Method	Effect
Miniature micro-grooved heat pipe	(Chien et al., 2003) [6]	Au-water (17 nm, 0.1%)	Experimental	+
	(Wei et al., 2005) [7]	Ag-water (10 nm, 0.01%)	Experimental	+
	(Kang et al., 2006) [8]	Ag-water (35 nm, 0.01%)	Experimental	+
	(Yang et al., 2008) [9]	CuO-water (50 nm, 1.0%)	Experimental	+
	(Liu and Lu, 2009) [10]	CNT-water (diameter: 15 nm, 2.0%)	Experimental	+
	(Do and Jang, 2010) [11]	Al_2O_3-water (38.4 nm, 0.8%)	Numerical	+
	(Shafahi et al., 2010) [12]	CuO-water, Al_2O_3-water, TiO_2-water	Numerical	+
	(Shafahi et al., 2010) [13]	CuO-water,Al_2O_3-water, TiO_2-water	Experimental	+
	(Liu et al., 2010) [14]	CuO-water (50 nm, 1.0%)	Experimental	+
	(Wang et al., 2010) [15]	CuO-water (50 nm, 1.0%)	Numerical	+
	(Alizad et al., 2012) [16]	CuO-water, Al_2O_3-water, TiO_2-water		
Mesh wick heat pipe	(Tsai et al., 2004) [17]	Au-water (21 nm)	Experimental	+
	(Liu et al., 2008) [18]	CuO-water (50 nm, 1.0%)	Experimental	
	(Chen et al., 2008) [19]	Ag-water (35 nm, 0.01%)	Experimental	
	(Asirvatham et al., 2013) [20]	Ag-water (59 nm, 0.009%)	Experimental	
	(Hung et al., 2013) [21]	Al_2O_3-water (20 nm, 1.0%)	Experimental	
	(Kole and Dey, 2013) [22]	Cu-water (122 nm, 0.5%)	Experimental	
	(Saleh et al., 2013) [23]	ZnO-ethylene glycol (23 nm, 0.5%)	Experimental	
	(Yousefi et al., 2013) [24]	Al_2O_3-water (35 nm, 0.5%)	Experimental	
	(Wang et al., 2012) [25]	CuO-water (50 nm, 1.0%)	Experimental	
	(Shukla et al., 2010) [26]	Cu-water (80 nm, 0.1%)	Experimental	
	(Do et al., 2010) [27]	Al_2O_3-water (30 nm, 2.4%)	Numerical	
	(Liu et al., 2011) [28]	CuO-water (50 nm, 1.0%)	Numerical	
	(Hameed and Rageb, 2014) [29]	Al_2O_3-water (35 nm, 5.0%)		
	(Solomon and Ramachandran, 2014) [30]	CuO-water (0.1%)		
Sintered metal wick heat pipe	(Kang et al., 2009) [31]	Ag-water (10 nm, 0.01%)	Experimental	+
Oscillating heat pipe	(Moraveji et al., 2012) [32]	Al_2O_3-water (35 nm, 1.0%)	Experimental	+
	(Ma et al., 2006) [33]	Diamond-water (20 nm and 40 nm, 2.2%)	Experimental	+
Loop heat pipe	(Ma et al., 2006) [34]	Diamond-water (20 nm and 40 nm, 2.2%)	Experimental	+
	(Shang et al., 2007) [35]	Cu-water (25 nm, 0.45%)	Experimental	+
	(Lin et al., 2008) [36]	Ag-water (20 nm, 0.1%)	Experimental	+
	(Park and Ma, 2007) [37]	CuNi-water (40–150 nm, 8.8 %)	Experimental	+
	(Qu et al., 2010) [38]	Al_2O_3-water (56 nm, 0.9%)	Experimental	+
	(Qu and Wu, 2011) [39]	Al_2O_3-water (200 nm, 0.9%)	Experimental	+
	(Karthikeyan et al., 2014) [40]	SiO2-water (200 nm, 0.6%)	Experimental	−
	(Riehl, 2006) [41]	Cu-water (70 nm, 0.5%)	Experimental	+
	(Wan et al., 2015) [42]	Ag-water (60 nm, 0.5%) Ni-water (40 nm, 3.5%) Cu-water (50 nm, 1.5%)		

("+" means heat transfer enhancement, "–" means heat transfer reduction).

2. Materials and methods

2.1. The experimental setup

The schematic diagram of experimental setup for LHP under investigation is shown in Fig. 1(a). The main function of this experiment rig is to determine the thermal performance of LHP charged with SiO_2–H_2O nanofluid with mass concentration ranged from 0 to 3% as a working fluid. The LHP shown in Fig. 1 installed with a power supply (W5 Series 30A-720A) and a flat evaporator, which is combined with the compensation chamber, with a total dimension of 50 mm × 50 mm × 4 mm. A water tank with 0.75 liter glass vessel equipped by drain valve is used as liquid reservoir. The whole LHP is made of copper. The internal and external diameters of both vapor and liquid lines are 13.5 mm and 15 mm, respectively, as illustrated in Fig. 1(b). The condenser section is made of 50 aluminum rectangular fins and cooled by installing two pieces of long screwed fans. The cross-section of condenser with fins are shown in Fig.1(c). To maintain steady state cooling conditions in the condenser section, the temperature and flow rate of the cooling liquid are fixed at constant value. To minimize the heat loss, the whole LHP is insulated by using glass wool. A copper block with heat rods inside is used to simulate the heat source, and the contact area between the evaporator and the heat source is 50 mm × 50 mm. In this experiment, the K-type thermocouples with an accuracy of $\pm 1.1\ ^{\circ}C$ are installed on the pipe/wall in different locations of the loop, including the copper base plate (T_B), the evaporator (T_E), the vapor line (T_V), the condenser section (T_C) and the liquid line (T_L). The temperatures measured by the thermocouples are collected through a data acquisition (Agilent 34970A) with sample rate of 1 Hz and connected to a PC to collect the data. The experiments are conducted under a heat input ranged from 20 W to 60 W by

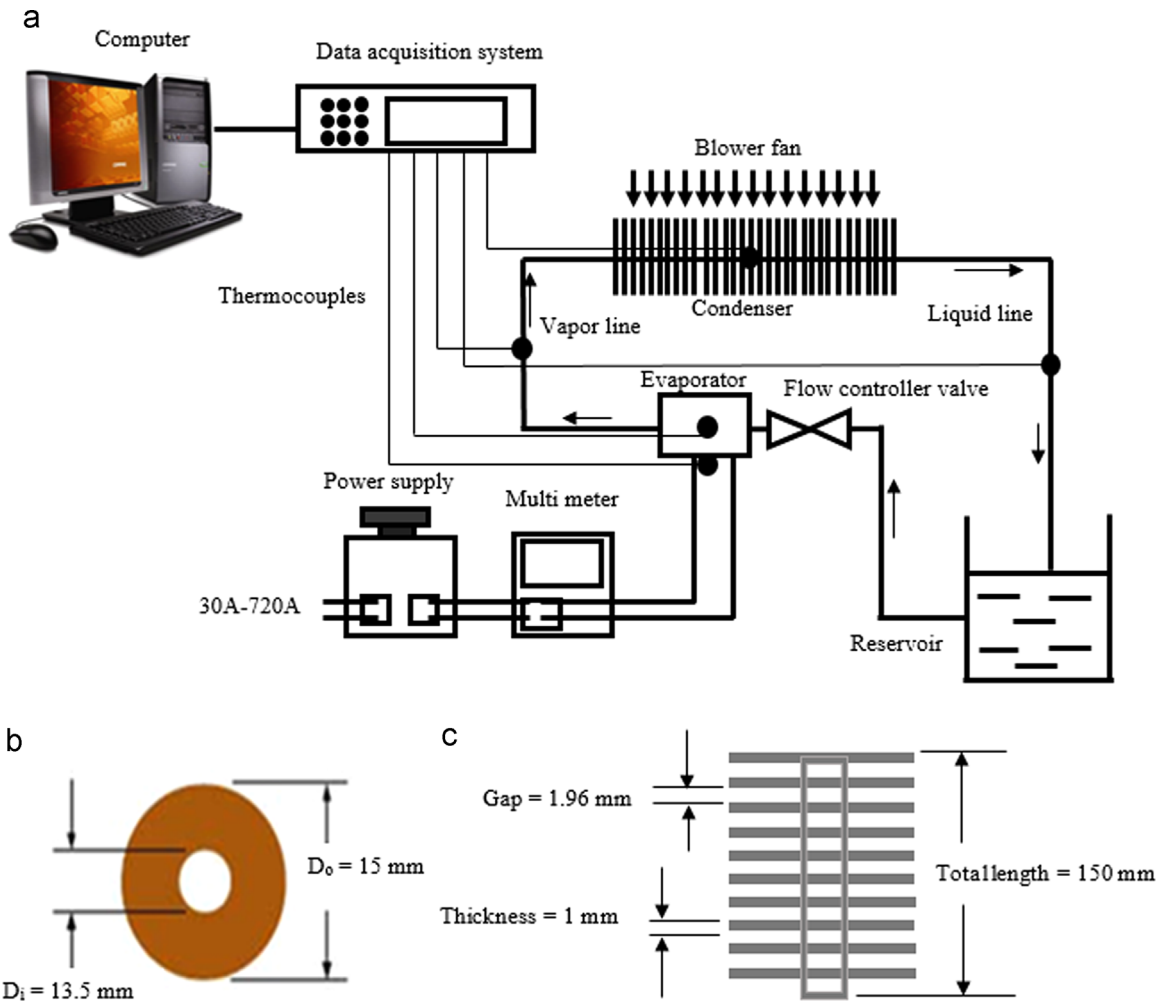

Fig. 1. (a) Schematic diagram of experimental apparatus. (b) Cross-section of heat pipe. (c) Cross-section of condenser with fins.

Table 2
Spécification of LHP.

Specification	Dimension/material
Evaporator (Flat)	
Dimension (mm)	L50 × W50 × H4
Material	Copper
Reservoir	
Volume (L)	0.75
Dimension (mm)	L149 × W100 × H85
Material	Aluminum faceplate
Vapor line	
Outer diameter, D_o (mm)	15
Inner diameter, D_i (mm)	13.5
Length (mm)	500
Material	Copper
Liquid line	
Outer diameter (mm)	15
Inner diameter (mm)	13.5
Length (mm)	500
Material	Copper
Condenser	
Dimension (mm)	L150 × W100 × H1
Material	Aluminum

Fig. 2. A photographic view of the SiO_2 nanoparticles.

adjusting the Variac. The airflow velocity is fixed as 4 m/s and the Reynolds number is varied from 1 to 20 by changing the coolant flow rate, controlled by adjusting the flow control valve. All the sensors are adjusted according to the desired heat input and Reynolds number. The specifications of the LHP are listed in Table 2.

2.2. Nanofluid preparation

In the present work, deionized water (DI-water) is taken as the base fluid for preparation of nanofluids in a Digital Ultrasonic Cleaner TJ001. Nanoparticles (Nanopowder) were purchased from Alfa Aesar Corp., Ward Hill, MA and blended with deionized water without any surfactant. The nanoparticles used in the present experiments are silica dioxide (SiO_2) with an average size of 12 nm and density of 2.65 g/cm^3. The photographic view of the nanoparticles as seen by the naked eyes is shown in Fig. 2. To make a desired percent mass concentration of nanofluids, the weights of deionized water and nanoparticles were measured by a sensitive balance (Ohaus Adventurer Balances) with an accuracy of 0.1 mg. The mass concentration of the powder is calculated from the weight of dry powder using the density provided by the supplier and the total volume of the suspension. For an example, 2.65 g of SiO_2 nanoparticles, which is 1 ml based on the density provided by the vendor, were added to the 99 g (99 ml) of DI-water to make 1 percent mass concentration of SiO_2–H_2O nanofluid.

$$\%\ \text{mass concentration} = \frac{w_{np}}{w_{bf} + w_{np}} \times 100 \tag{1}$$

where

w_{np} = amount of nanoparticles in gram

w_{bf} = amount of base fluid in gram.

The nanofluid was then stirred by a magnetic stirrer for 5 h before undergoing ultrasonication process for one and a half

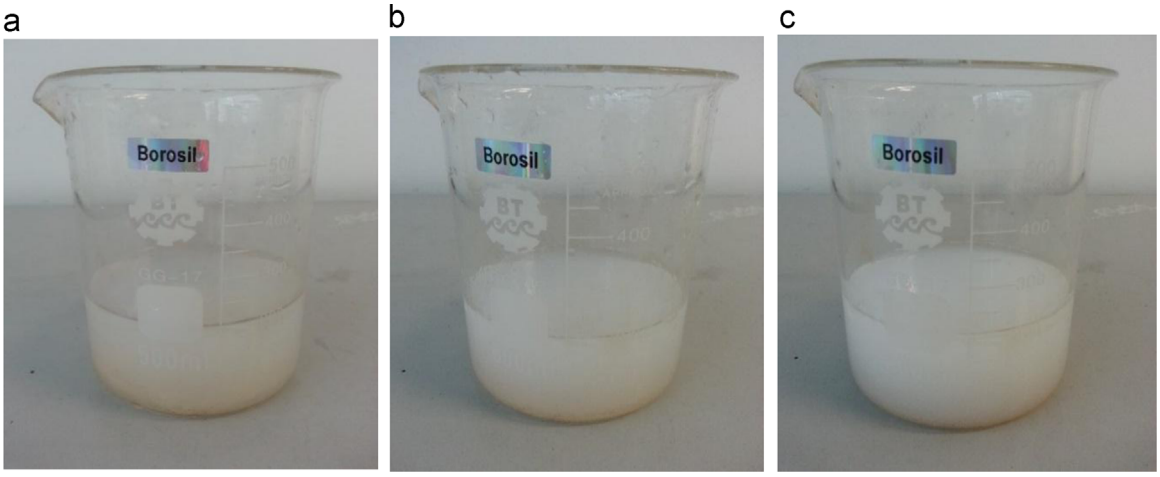

Fig. 3. SiO_2–H_2O nanofluid at (a) 0.5%, (b) 1% and (c) 3% of particle mass concentration after 30 days.

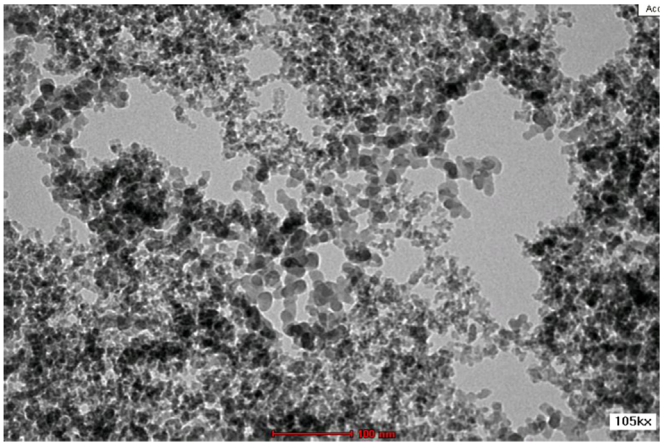

Fig. 4. TEM images of SiO_2 nanoparticles suspended in pure water.

hours. This is to ensure uniform dispersion of nanoparticles and also to prevent the nanoparticles from the aggregation in the nanofluids. Then, the SiO_2/DI-water mixture was ultrasonicated using an ultrasonic cleaner. The purpose of sonication was to vibrate the nanoparticles in the base fluid so that agglomerates of nanoparticles will break up forming a suspension of isolated nanoparticles. The mixtures were sonicated for 3 h continuously. The nanofluids were at significantly high temperature after the sonication. The nanofluids samples thus prepared are kept for observation and no particle settlement was observed at the bottom of the beaker containing nanofluids. The photographic view of nanofluid suspension prepared after magnetic stirring and sonication process is as shown in Fig. 3, which depicts a picture at different mass concentrations of SiO_2–H_2O nanofluids, respectively. Since no concentration gradient appears, the nanofluid employed here maintains stability for several weeks and hence surfactants are not mixed in the prepared nanofluids in present experiment. The nanofluids prepared are assumed to be an isentropic, Newtonian in behavior and their thermo physical properties are uniform and constant with time all through the fluid sample. Fig. 4 shows the transmission electronic microscope (TEM) images of the dispersed SiO_2 nanoparticles in water with particle mass concentration of 1% at magnification-105k × at room temperature.

2.3. Thermal analysis

The objective of the current study is to evaluate the total thermal resistance (R_{th}) of the LHP using SiO_2–H_2O nanofluid as working fluid for various heat inputs under steady state and transient conditions. The results obtained from experimental investigation used to verify by RSM model. The nanoparticle mass concentration that yields the minimum $R_{th}$is then found out, and the various steps to estimate R_{th} are as follows. The thermal resistance network of the system is shown in Fig. 5.

The heat flux ($\dot{q}$) that applied on the bottom of base plate can be expressed as

$$q = \frac{Q}{A_b} \tag{2}$$

where Q denotes the heat input and A_b is the area of base plate. The thermal resistances of the LHP are defined as [43] the thermal resistance between the copper base plate and the evaporator section (R_B) is

$$R_B = \frac{T_B - T_E}{Q} \tag{3}$$

where T_B denotes the temperature at the copper base plate and T_E is the temperature at the evaporator.

The thermal resistance of the evaporator section (R_E) is

$$R_E = \frac{T_E - T_V}{Q} \tag{4}$$

where T_V is the temperature at the vapor line.

Fig. 5. Thermal resistance network of LHP.

The thermal resistance of the vapor line (R_V) is

$$R_V = \frac{T_V - T_C}{Q} \tag{5}$$

where T_C is the temperature at the condenser section.

The convective thermal resistance of the condenser (R_C) is

$$R_C = \frac{T_C - T_L}{Q} \tag{6}$$

where T_L is the temperature at the liquid line.

The thermal resistance of the liquid line (R_L) is

$$R_L = \frac{T_L - T_A}{Q} \tag{7}$$

where T_A is the ambient temperature.

According to the thermal resistance network as shown in Fig. 5, the R_{th} of the system is given by

$$R_{th} = R_B + R_E + R_V + R_C + R_L \tag{8}$$

3. Experimental design and statistical analysis

In this study, experimental design of the operating conditions is performed by RSM which is a collection of mathematical and statistical techniques that are useful for the optimization of industrial processes, and widely used for experimental designs [44]. In this study, RSM is used to assess the relationship between response (R_{th}) and operating variables (nanoparticle mass concentration and heat input), in addition to optimize the operating variables to predict the best value of the response. Central Composite Design (CCD), the most commonly used approach of RSM, is utilized in this study. CCD allows reasonable amount of information to test lack of fit when an adequate number of experimental values exist [45]. CCD and RSM are established with the help of the Design-Expert 6.0.7 (Stat-Ease Inc., Minneapolis, MN) software program. The two significant independent variables considered are nanoparticle mass concentration (A) and heat input (B), as presented in Table 3. Each independent variable is varied over two levels. The low and high levels of each variable are designated as -1 and $+1$, respectively. The variable levels are selected based on the results obtained from preliminary experiments.

As there are only three levels for each factor, the appropriate model is an empirical second-order polynomial model (quadratic model) as indicated by Montgomery [46]. The quadratic model used is expressed as

$$Y = \beta_0 + \sum_{i=1}^{k} \beta x_i + \sum_{i=1}^{k} \beta_{ii} x_i^2 + \sum_{i=1} \sum_{i \neq j=1} \beta_{ij} x_i x_{ij} + \varepsilon \tag{9}$$

where Y is the predicted response; x_i and x_j are variables or independent factors; β_0 is the constant coefficient; β_j, β_{jj}, and β_{ij} are interaction coefficients of linear, quadratic, and the second-order terms, respectively; k is the number of independent variables (2) and ε is the error [46]. Analysis of variance (ANOVA) is employed for graphical analysis of the data to obtain the interaction between the variables and the response. The quality of the fit polynomial model is expressed by the coefficient of determination (R^2), and its statistical significance is confirmed through the student t test in the same software. Model terms are assessed by the P value (probability) with 95% confidence level. Three-dimensional plots and their particular contour plots are achieved based on effects of the operational variables at three levels.

The total number of experiments for the two factors is obtained as 13. Eight experiments are enhanced with five replications to assess the pure error. A total of 13 runs of the CCD experimental design and response are illustrated in Table 4 which illustrates the outcome of the experimental conditions as average of the triplicate tests achieved for each operating condition.

Table 3
Independent variables of the CCD design.

Level of value	A nanoparticle mass concentration (%)	B power input (W)
−1	0	20
1	1.0	60

Table 4
Response values for different experimental conditions.

Run no.	Factor *A* nanoparticle mass concentration (%)	Factor *B* heat input (W)	Response total thermal resistance (°C/W)
1	0.00	60	2.7998
2	0.50	40	3.2300
3	0.50	40	3.1885
4	0.00	40	3.3010
5	0.50	40	3.2270
6	0.50	20	3.4190
7	0.50	60	2.7054
8	0.50	40	3.1958
9	0.50	40	3.1825
10	0.00	40	3.6890
11	1.00	60	3.6875
12	1.00	20	3.6625
13	1.00	40	2.6645

4. Results and discussion

4.1. Effect of Reynolds number on R_{th}

Reynolds number has a strong influence on the thermal performance of nanofluid charged-LHP. Thus, it is necessary to identify the suitable Reynolds number for the LHP charged with nanofluid in order to achieve maximum heat transfer performance. Fig. 6 shows the relationship of total thermal resistance (R_{th}) of 1% SiO_2–H_2O-charged LHP at various Reynolds numbers for different applied heat inputs. The Reynolds number is varied by changing the flow rate of liquid. The flow rate of liquid is controlled by flow control valve. It is observed that the increase of Re from 1 to 10 leads to decrease in R_{th} of the LHP, while the thermal performance of the LHP is deteriorated when the Re changed from 10 to 20 for all the applied heat inputs. At Re of 20, it is observed in present study that the liquid flow too fast in the pipe, which leads to poor heat transport capability and reduces the bubble formation. This is due to the fact that, with increase in Reynolds number which leads to increase the fluid velocity, bubble formation rate decreases and subsequently diffusion of dissolved vapor phase into bubbles does not occur completely and therefore, bubbles does not have enough time to reach to their maximum size and leaves the heating surface sooner. Thus, there is an optimal Reynolds number, which is about 10 for the LHP charged with SiO_2–H_2O nanofluid in the present experiment. Hence, the Reynolds number of 10 is employed throughout the entire study as the experimental results show that this value yields the best thermal performance.

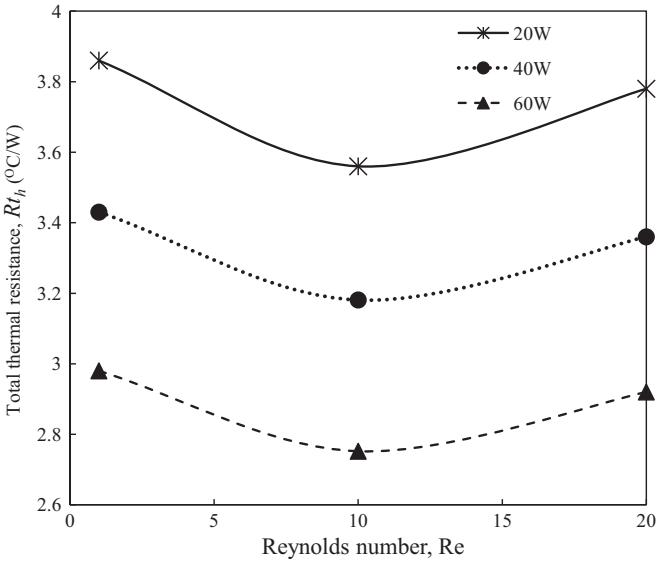

Fig. 6. Influence of Reynolds number on the R_{th} of LHP charged with SiO_2 nanoparticle mass concentration of 1% for various heat inputs.

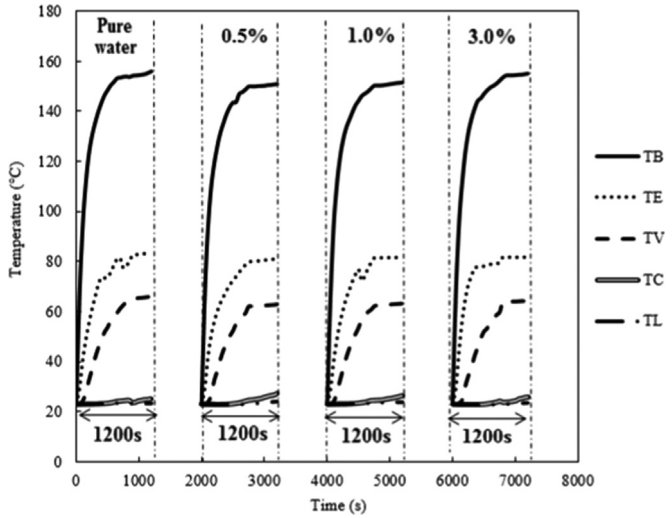

Fig. 7. Influence of nanoparticle mass concentrations on transient wall temperature distribution of LHP for SiO_2–H_2O nanofluid under 60 W.

4.2. Transient temperature distribution

Fig. 7 illustrates the transient wall temperature distribution of LHP charged with SiO_2–H_2O nanofluid at different mass concentrations, which includes 0% (pure water), 0.5%, 1% and 3% under a heat input of 60 W. At the concentration of 0%, the temperatures of all points gradually increase until 900 s and become steady thereafter. For particle mass concentrations of 0.5%, 1% and 3%, the temperatures of all points gradually rise and the steady state is achieved at first 800 s, which reach their steady state faster than pure water in difference of 100 s. For particle mass concentration of 3%, the temperatures at evaporator side of LHP in both transient and steady states, which includes the temperature of the base (T_B), evaporator (T_E) and vapor line (T_V) are slightly higher than 0.5% and 1% but still lower than pure water. The maximum reduction in evaporator wall temperature is about 4 °C, is attained at the particle mass concentration of 0.5% as compared with pure water. The validity of the present experimental results is also proved with Wan et al. [42] results, where the LHP charged with nanofluid yields lower wall temperature and reaches its steady state faster than LHP charged with pure water.

4.3. Effects of nanoparticle mass concentration and heat input on R_{th}

Fig. 8 shows the relationship between the R_{th} and nanoparticle mass concentration for various heat input. As depicted in

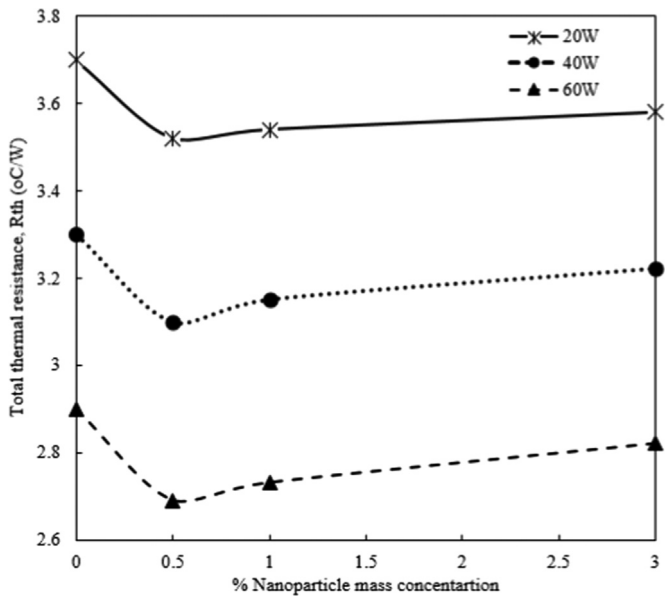

Fig. 8. Influence of SiO_2 nanoparticle mass concentrations on the R_{th} of LHP for various heat inputs.

Table 5
Summary of R_{th} at various nanoparticle mass concentrations and heat inputs.

	R_{th}			
Q (W)	0%	0.50%	1%	3%
20	3.716	3.515	3.560	3.601
40	3.311	3.121	3.181	3.203
60	2.859	2.692	2.752	2.802

Fig. 8, the R_{th} decreased up to 0.5% and increased on further increase in nanoparticle mass concentration (from 0.5% to 1%) at all heat inputs. Thus, there is an optimal particle concentration, which is about 0.5% for the SiO_2–H_2O-charged LHP in the present experiment. Thus, the addition of silica nanoparticles to base water with high mass concentration deteriorated the thermal performance of the LHP due to the depositions with larger particle agglomerates appeared at the evaporator as reported by Qu and Wu [39]. At the optimal mass concentration of 0.5%, the maximum reduction in R_{th} of SiO_2–H_2O-charged LHP is about 2.702 °C/W (or 5.5%) under heat input of 60 W, is obtained as compared with pure water (0% nanoparticle mass concentration) charged LHP. It is clear from the Fig. 8 that when the heat input increases, the thermal resistance decreases and the nanoparticle mass concentration has a great impact on the R_{th}. Table 5 summarizes the changes in R_{th} with nanoparticle mass concentration and heat input.

4.4. Analysis of variance

Table 6 demonstrates the ANOVA of regression parameters of the predicted response surface quadratic model. The model for R_{th} is found to be significant using the t test at 5% significance level ($P < 0.05$). The F value of 75.65 of the model and its low probability value indicate that the model is significant for R_{th} ($F > 0.10$ shows that the model terms are insignificant). As shown in Table 6, the "Adequate Precision" ratio of the model is 25.977 (Adequate Precision > 4), which is an adequate signal for the model [47]. The value of coefficient of determination ($R^2 = 0.9818$) obtained for R_{th} is above 0.80, showing that only 1.82% (1–0.9818) of the total dissimilarity might not be explained by the empirical model. For a high-quality fit of a model, the coefficient of determination should be more than 0.80 [46]. High R^2 value demonstrates excellent conformity between the calculated and observed results within the range of experiment. In this study, A, B, A^2, and B^2 are significant model terms. Insignificant model terms having limited weights, such as AB, is excluded from the study in order to get better model [46]. The response surface model created for predicting R_{th} has been considered sensible. The final regression model, in terms coded factors, is expressed by the following second-order polynomial equation:

$$R_{th} = +3.71472 - 0.42017A - 0.00148548B + 0.44821A^2 - 0.000273681B^2 \quad (10)$$

By concerning the diagnostic plots provided by the software, such as normal probability plots of the studentized residuals, as well as the predicted versus actual value plots, the model validity could be judged. Fig. 9 shows the normal probability plots of the studentized residuals for R_{th}. A normal probability plot demonstrates whether the residuals follow a normal distribution; in this case, it can be assumed that the data is normally distributed. The assessment of actual and predicted values of R_{th} is shown in Fig. 10. Actual values are the measured response data for a particular run, and the predicted values are evaluated from the model and generated by using the approximating functions. The agreement between the actual and predicted values of R_{th} is satisfactory and in agreement with the statistical significance of the quadratic model presented in Table 5.

Table 6
ANNOVA for analysis of variance and adequacy of the quadratic model.

Source	Sum of squares	d.f.	Mean square	F Value	$P > F$
Model	1.16	5	0.23	75.65	< 0.0001
A	5.01E-003	1	5.01E-003	1.63	0.0142
B	1.11	1	1.11	360.06	< 0.0001
A^2	0.035	1	0.035	11.27	0.0121
B^2	0.033	1	0.033	10.76	0.0135
AB	1.84E–003	1	1.84E–003	0.6	0.4644
Residual	0.022	7	3.08E–003		
Lack of fit	0.020	3	6.52E–003	13.22	< 0.0001
Pure error	1.97E–003	4	4.93E–004		

SD = 0.055, mean = 3.20, C.V = 1.74, $R^2 = 0.9818$, $R^2_{adj} = 0.9689$, Adeq. precision = 25.977.

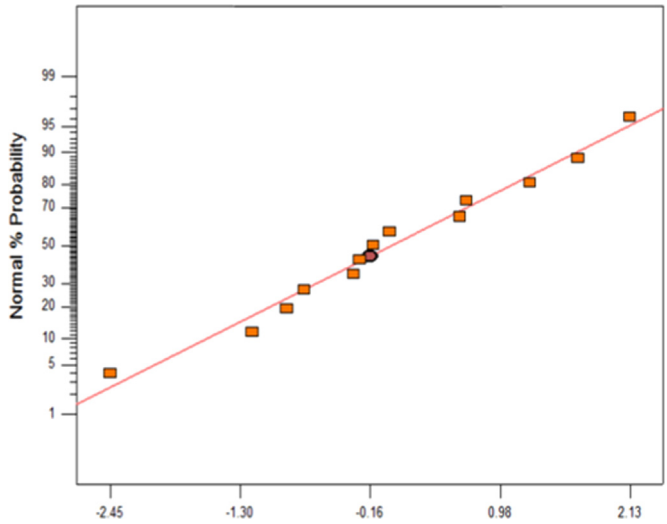

Fig. 9. Normal probability plot of studentized residuals actual.

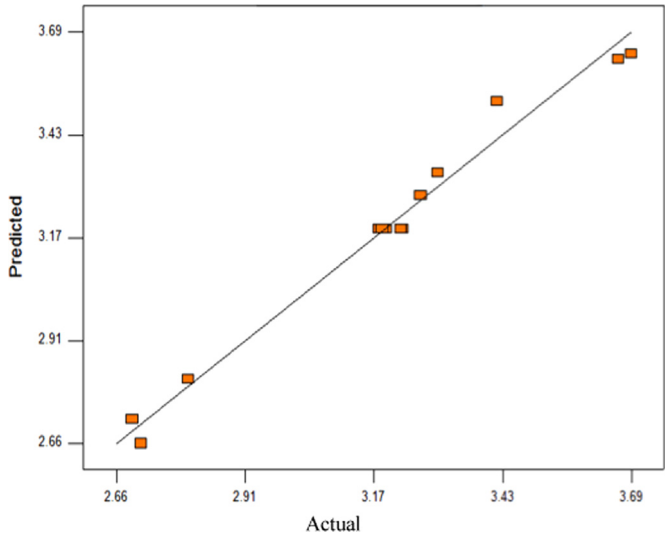

Fig. 10. Predicted versus actual values of R_{th}.

4.5. Interaction between variables and optimization

Eq. 10 is used to visualize the influences of operating variables (i.e., nanoparticle mass concentration and heat input) on R_{th} (Fig. 11). The curvature of 3D surfaces indicates that the nanoparticle mass concentration and heat input have major effect on R_{th}; increasing the nanoparticle mass concentration up to about 0.5% leads to decrease in R_{th} and then begins to increase, while the increasing of the heat input also leads to significant decrease in R_{th}.

The results are optimized via Design-Expert software. In numerical optimization, nanoparticle mass concentration and heat input are goaled to be in range, R_{th} is aimed to be minimized. At the optimized conditions, nanoparticle mass concentration of 0.48% and heat input of 59.97 W, R_{th} being 2.66 °C/W which is predicted based on desirability function of 1.00. To verify the accuracy of the predicted model and the consistency of the optimum combination, an additional run is conducted under optimal conditions based on the results from the model. The results show that the model prediction for the R_{th} is very close to the actual experimental results (Table 5). These results confirm that RSM is a powerful tool for optimizing the operational conditions for minimum R_{th} of LHPs.

5. Conclusion

The experimental design and optimization of operating conditions of LHP for desktop PC cooling is accomplished with

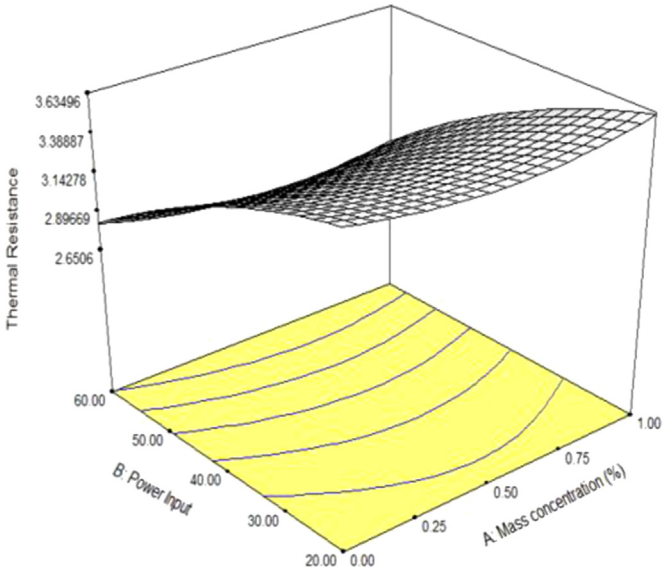

Fig. 11. 3D surface plots of Rth as function of nanoparticle mass concentration (A) and heat input (B).

RSM. The independent variables are nanoparticle mass concentration and heat input, and the objective function is total thermal resistance (to minimize). Results show that the nanoparticle mass concentration and the heat input are crucial on the R_{th}. The results are optimized via Design-Expert software and found that a nanoparticle mass concentration of 0.48% and heat input of 59.97 W could produce the minimum R_{th} (2.66 °C/W). This study may be extended for more variables such as other types of nanoparticles mass concentration and geometrical parameters such as the diameter, shape and length of LHP in designing more efficient nanofluid-charged LHPs.

Acknowledgments

The authors would like to sincerely thank the Ministry of Higher Education (MOHE) of Malaysia for the provision of a grant with code no. 20120228FRGS to support this work.

References

[1] L. Fedele, L. Colla, S. Bobbo, S. Barison, F. Agresti, Experimental stability analysis of different water-based nanofluids, Nanoscale Res. Lett. 6 (2011) 300–308.
[2] G. Huminic, A. Huminic, Application of nanofluids in heat exchangers: a review, Renew. Sust. Energy Rev. 16 (2012) 5625–5638.
[3] S. Halelfadl, A.M. Adham, N. Mohd-Ghazali, T. MareP. EstelleR. Ahmad, Optimization of thermal performances and pressure drop of rectangular microchannel heat sink using aqueous carbon nanotubes based nanofluid, Appl. Therm. Eng. 62 (2014) 492–499.
[4] H.R. Seyf, M. Feizbakhshi, Computational analysis of nanofluid effects on convective heat transfer enhancement of micro-pin-fin heat sinks, Int. J. Therm. Sci. 58 (2012) 168–179.
[5] M.R. Hajmohammadi, H. Maleki, G. Lorenzini, S.S. Nourazar, Effects of Cu and Ag nano-particles on flow and heat transfer from permeable surfaces, Adv. Powder Technol. 26 (2015) 193–199.
[6] H.T. Chien, C.Y. Tsai, P.H. Chen, P.Y. Chen, Improvement on thermal performance of a disk-shaped miniature heat pipe with nanofluid, in: Proceedings of the Fifth International Conference on Electronic Packaging Technology, IEEE, Shanghai, China, 2003, pp. 389–391.
[7] W.C. Wei, S.H. Tsai, S.Y. Yang, S.W. Kang, Effect of nano-fluid concentration on heat pipe thermal performance, IASME Trans. 2 (2005) 1432–1439.
[8] S.W. Kang, W.C. Wei, S.H. Tsai, S.Y. Yang, Experimental investigation of silver nano-fluid on heat pipe thermal performance, Appl. Therm. Eng. 26 (2006) 2377–2382.
[9] X.F. Yang, Z.H. Liu, J. Zhao, Heat transfer performance of a horizontal micro grooved heat pipe using CuO nanofluid, J. Micromech. Microeng. 18 (2008) 35–38.
[10] Z.H. Liu, L. Lu, Thermal performance of axially microgrooved heat pipe using carbon nanotube suspensions, J. Thermophys. Heat. Transf. 23 (2009) 170–175.
[11] K.H. Do, S.P. Jang, Effect of nanofluids on the thermal performance of a flat micro heat pipe with a rectangular grooved wick, Int. J. Heat. Mass. Transf. 53 (2010) 2183–2192.
[12] M. Shafahi, V. Bianco, K. Vafai, O. Manca, Thermal performance of flat-shaped heat pipes using nanofluids, Int. J. Heat. Mass. Transf. 53 (2010) 1438–1445.
[13] M. Shafahi, V. Bianco, K. Vafai, O. Manca., An investigation of the thermal performance of cylindrical heat pipes using nanofluids, Int. J. Heat. Mass. Transf. 53 (2010) 376–383.
[14] Z.H. Liu, Y.Y. Li, R. Bao, Thermal performance of inclined grooved heat pipes using nanofluids, Int. J. Therm. Sci. 49 (2010) 1680–1687.
[15] G.S. Wang, B. Song, Z.H. Liu, Operation characteristics of cylindrical miniature grooved heat pipe using aqueous CuO nanofluids, Expt. Therm. Fluid Sci. 34 (2010) 1415–1421.
[16] K. Alizad, K. Vafai, M. Shafahi, Thermal performance and operational attributes of the startup characteristics of flat-shaped heat pipes using nanofluids, Int. J. Heat. Mass. Transf. 55 (2012) 140–155.

[17] C.Y. Tsai, H.T. Chien, P.P. Ding, B. Chan, T.Y. Luh, P.H. Chen, Effect of structural character of gold nanoparticles in nanofluid on heat pipe thermal performance, Mater. Lett. 58 (2004) 1461–1465.
[18] Z.H. Liu, T. Shu, Application of nanofluids in thermal performance enhancement of horizontal screen heat pipe, J. Aerosp. Power 23 (2008) 1623–1627.
[19] Y.T. Chen, W.C. Wei, S.W. Kang, C.S. Yu, Effect of nanofluids on flat heat pipe thermal performance, in: Proceedings of the 24th IEEE Semiconductor Thermal Measurement and Management Symposium, 2008, IEEE, San Jose, CA, USA, pp. 16–20.
[20] L.G. Asirvatham, R. Nimmagadda, S. Wongwises, Heat transfer performance of screen mesh wick heat pipes using silver–water nanofluid, Int. J. Heat. Mass. Transf. 60 (2013) 201–209.
[21] Y.H. Hung, T.P. Teng, B.G. Lin, Evaluation of the thermal performance of a heat pipe using alumina nanofluids, Exp. Therm. Fluid Sci. 44 (2013) 504–511.
[22] M. Kole, T.K. Dey, Thermal performance of screen mesh wick heat pipes using water-based copper nanofluids, Appl. Therm. Eng. 50 (2013) 763–770.
[23] R. Saleh, N. Putra, S. Purbo Prakoso, W. Nata Septiadi, Experimental investigation of thermal conductivity and heat pipe thermal performance of ZnO nanofluids, Int. J. Therm. Sci. 63 (2013) 125–132.
[24] T. Yousefi, S.A. Mousavi, B. Farahbakhsh, M.Z. Saghir, Experimental investigation on the performance of CPU coolers: Effect of heat pipe inclination angle and the use of nanofluids, Microelectron. Reliab. 53 (2013) 1954–1961.
[25] P.Y. Wang, X.J. Chen, Z.H. Liu, Y.P. Liu, Application of nanofluid in an inclined mesh wicked heat pipes, Thermochim. Acta 539 (2012) 100–108.
[26] K.N. Shukla, A.B. Solomon, B.C. Pillai, M. Ibrahim, Thermal performance of cylindrical heat pipe using nanofluids, J. thermophys. Heat. Transf. 24 (2010) 796–802.
[27] K.H. Do, H.J. Ha, S.P. Jang, Thermal resistance of screen mesh wick heat pipes using the water-based Al_2O_3 nanofluids, Int. J. Heat. Mass. Transf.53 (25–26) (2010) 5888–5894.
[28] Z.H. Liu, Q.Z. Zhu, Application of aqueous nanofluids in a horizontal mesh heat pipe, Energy Convers. Manag. 52 (1) (2011) 292–300.
[29] H.G. Hameed, A.M. Rageb, Numerical simulation of thermal performance of constant conductance cylinder heat pipe using nanofluid, Al-Qadisiya J. Eng. Sci. 7 (2014) 343–365.
[30] (a) A.B. Solomon, K. Ramachandran, B.C. Pillai, Thermal performance of a heat pipe with nanoparticles coated wick, Appl. Therm. Eng. 36 (2012) 106–112;
(b) T.S. Swanson, G.C. Birur, NASA thermal control technologies for robotic spacecraft, Appl. Therm. Eng. 23 (2003) 1055–1065.
[31] S.W. Kang, W.C. Wei, S.H. Tsai, C.C. Huang, Experimental investigation of nanofluids on sintered heat pipe thermal performance, Appl. Therm. Eng. 29 (2009) 973–979.
[32] M.K. Moraveji, S. Razvarz, Experimental investigation of aluminum oxide nanofluid on heat pipe thermal performance, Int. Commun. Heat. Mass. Transf. 39 (2012) 1444–1448.
[33] H.B. Ma, C. Wilson, B. Borgmeyer, K. Park, Q. Yu, U.S. Choi, M. Tirumala, Effect of nanofluid on the heat transport capability in an oscillating heat pipe, Appl. Phys. Lett. 88 (2006) 143116.
[34] H.B. Ma, C. Wilson, Q. Yu, K. Park, U.S. Choi, M. Tirumala, An experimental investigation of heat transport capability in a nanofluids oscillating heat pipe, J. Heat. Transf. 128 (2006) 1213–1216.
[35] F.M. Shang, D.Y. Liu, H.Z. Xian, Y.P. Yang, X.Z. Du, Flow and heat transfer characteristics of different forms of nanometer particles in oscillating heat pipe, J. Chem. Indust. Eng. 58 (9) (2007) 2200–2204.
[36] Y.H. Lin, S.W. Kang, H.L. Chen, Effect of silver nanofluid on pulsating heat pipe thermal performance, Appl. Therm. Eng. 28 (2008) 1312–1317.
[37] K. Park, H.B. Ma, Nanofluid effect on heat transport capability in a well-balanced oscillating heat pipe, J. Thermophys. Heat. Transf. 21 (2007) 443.
[38] J. Qu, H.Y. Wu, P. Cheng, Thermal performance of an oscillating heat pipe with Al_2O_3–water nanofluids, Int. Commun. Heat. Mass. Transf. 37 (2010) 111–115.
[39] J. Qu, H.Y. Wu, Thermal performance comparison of oscillating heat pipes with SiO_2/water and Al_2O_3/water nanofluids, Int. J. Therm. Sci. 50 (2011) 1954–1962.
[40] V.K. Karthikeyan, K. Ramachandran, B.C. Pillai, A. Brusly Solomon, Effect of nanofluids on thermal performance of closed loop pulsating heat pipe, Exp. Therm. Fluid Sci. 54 (2014) 171–178.
[41] R.R. Riehl, Analysis of loop heat pipe behavior using nanofluid, in: Proceedings of Heat Powered Cycles International Conference (HPC), September 11–14, 2006, New Castle, UK.
[42] Z. Wan, J. Deng, B. Li, Y. Xu, X. Wang, Y. Tang, Thermal performance of a miniature loop heat pipe using water–copper nanofluid, Appl. Therm. Eng. 78 (2015) 712–719.
[43] G. Franchi, X. Huang, Development of composite wicks for heat pipe performance enhancement, Heat Transf. Eng. 29 (2008) 873–884.
[44] D. Bas, I.H. Boyaci, Modeling and optimization in usability of Response Surface Methodology (RSM), J. Food Eng. 78 (2007) 836–845.
[45] M.J.K. Bashir, H.A. Aziz, M.S. Yusoff, M.N. Adlan, Application of Response Surface Methodology (RSM) for optimization of ammoniacal nitrogen removal from semi-aerobic landfill leachate using ion exchange resin, Desalination 254 (2010) 154–161.
[46] D.C. Montgomery, Design and analysis of experiments, 7th Edition, John Wiley & Sons, Inc., New York, 2008.
[47] Design-Expert Software Trial Version 6.0.7, User's guide, 2008.